Wireless Pers Commun (2013) 71:2295–2312
DOI 10.1007/s11277-012-0936-4

De-noising of GPS Receivers Positioning Data Using Wavelet Transform and Bilateral Filtering

M. R. Mosavi · I. EmamGholipour

Published online: 21 November 2012

Abstract The need for precise position and navigation aids in many areas of industry is becoming increasingly apparent. There are many errors associated with the navigation solution of the global positioning system (GPS), including satellite ephemeris error, satellite clock error, ionospheric delay, tropospheric delay, multipath, receiver measurement error and selective availability (SA). Noise can create an error between centimeters to several meters. In this paper, the proposed technique applied to smooth noise for GPS receiver positioning data is based upon the analysis of wavelet transform (WT), bilateral filter (BF) and diffusivity function. The WT is a powerful tool of signal processing for its multiresolutional possibilities. BF is a local, non-linear and non-iterative technique. It is applied to approximation subband. We decompose a GPS positioning data into low-frequency and high-frequency components and apply BF on the approximation coefficients and diffusivity function on the detail coefficients at each decomposition level for data smoothing. A single-frequency and low-cost commercial GPS receiver manufactured by Rockwell Company is used to test our method. The experimental results on measurement data demonstrate the effectiveness of the proposed method; so that the total root mean square (RMS) error reduces to less than 0.29 m with SA on and 0.15 m with SA off using Daubechie wavelet.

Keywords Noise smoothing · GPS · Wavelet transform · Bilateral filter · Diffusivity function

1 Introduction

Simple autonomous GPS receivers have become ubiquitous in both military and civilian applications for instantaneous location services. The simplest positioning systems use the

M. R. Mosavi (✉) · I. EmamGholipour
Department of Electrical Engineering, Iran University of Science and Technology,
Narmak,
Tehran 16846-13114, Iran
e-mail: m_mosavi@iust.ac.ir

I. EmamGholipour
e-mail: i_emamgholipour@elec.iust.ac.ir

unencrypted L1 band (1575.42 MHz) and lowest resolution Coarse/Acquisition (C/A) mode protocol [1]. A GPS receiver determines its position by estimating the distance of receiver from each of several visible satellites. The position of satellites is determined from the transmitted ephemeris. The distance is determined by estimating the propagation time delay of the transmitted code. With the position of satellites established and the distance of receiver to each satellite estimated, the position of receiver can be established by triangulation methods [2].

In GPS, distances between the receiver and satellites are measured. The distance is called Pseudo-Range (PR). PRs, $r_i (i = 1, 2, \ldots, n)$, are simply represented as follows [3]:

$$r_i = \sqrt{(x_{si} - x)^2 + (y_{si} - y)^2 + (z_{si} - z)^2} + s \tag{1}$$

In the above equation, (x_s, y_s, z_s) is satellite's coordinate calculated by information which is called ephemeris, (x, y, z) is receiver's coordinate, s is receiver's clock offset converted into length, n is the number of available satellites and subscript i indicates satellite's number. In order to measure a position by GPS, observing more than three satellites are needed since not only the receiver' coordinates, but also the receiver's clock offset must be calculated. PR can be computed by measuring the satellite signal propagation time τ_i using $r_i = c\tau_i$, where is the propagation speed of radio signal [4]. The receiver uses precise time and satellite position data, along with other information in the transmitted signals, to calculate position coordinates. The time that it takes the signal to travel from the satellite to receiver is one of the critical values that the receiver must calculate. There are a number of errors that affect the position estimates derived from GPS measurements. The errors can generally be divided into three distinct groups: satellite dependent errors, receiver dependent errors and propagation dependent errors [5].

Real world signals are often corrupted by noise which may severely limit their usefulness. For this reason, signal de-noising is a topic that continually draws great interest. Wavelet transforms (WTs) have gained wide acceptance as a valuable tool for common signal processing tasks. In reality, the signal for a long time is non-stationary and its frequency changes at any time. The change can be divided into the slow and quick change: the slow corresponds to the low-frequency of the non-stationary signal and represents the main outline of signal; the quick corresponds to the high-frequency and represents the detail. The energy of the signal mainly concentrates on the low and is relatively low in the high [6].

Bilateral Filter (BF), representing a large class of non-linear filters proposed by Tomasi et al. [7], is a non-iterative and local approach to sharp feature-preserving smoothing. The BF is used to smooth out noise while maintaining sharp feature detail by being more selective in the samples allowed to contribute to the weighted sum. The filter works by replacing the current value of a focal sample with the bilaterally weighted sum of samples in its immediate area. The bilateral weights are calculated such that samples on the same side of a sharp feature contribute to the new focal sample value, while those on the opposing side effectively do not contribute, thus helps in maintaining the sharp features [8].

Smoothing filters in GPS can be partitioned into two groups: position domain filters and range domain filters. Position domain filtering (filtering in the state space) always shows better performance than range domain filtering (filtering in the measurement space) [9].

Extending the range domain filter introduced by [10], position domain filters have been subsequently introduced. The six most representative among these are the complementary filter proposed by [11], the phase-connected filter proposed by [12], a positioning filter with phase smoothing in the position domain proposed by [13], the stepwise unbiased position projection filter proposed by [14], the efficient kinematic position domain filter proposed by

[15], and a bank of extended Kalman filters followed using a Gaussian sums non-linear filter proposed by [16].

All of above mentioned methods require to differential GPS (DGPS) and extra sensors that make them expensive for implementation. In this paper, a new method for noise smoothing of GPS receiver positioning data using wavelet analysis WT and BF is proposed without DGPS and extra sensors. This paper is organized as follows. Next section describes the GPS error sources briefly. The wavelet de-noise fundamental principle is introduced in Sect. 3. In Sect. 4, we will propose an extension of the BF. Simulations and experiments results with real data are discussed in Sect. 5. Finally, Sect. 6 reports conclusion.

2 GPS Error Sources

GPS errors are subdivided into the six following classes: satellite orbit errors, satellite clock error, receiver clock error, tropospheric delay, ionospheric delay and multipath [17]. The ephemeris parameters in navigation message will not exactly describe the satellite's true orbit; therefore satellite orbit errors are produced. Satellite clock error is caused by the inability of the satellite's oscillator (clock) to maintain the GPS system reference time frame. A GPS receiver has one oscillator which generates all internal signals required to track the GPS constellation. Thus, if the receiver clock is in error, the error will affect measurements to all satellites being tracked by the same amount. In other words, the receiver clock error is identical for all satellites observed simultaneously. The receiver clock error is generally larger than the satellite clock error. The troposphere is loosely defined as the region of the earth's atmosphere below an altitude of 50 km. This portion of the atmosphere causes a delay on PR and carrier phase measurements. The ionosphere is the portion of the atmosphere between an altitude of 50 and 1000 km in which free thermal electrons are present. As the GPS signal passes through the ionosphere, the PR is retarded, but the carrier phase is advanced. The magnitude of the ionospheric advance in the carrier is the same as the magnitude of its delay in the PR [18].

Multipath error happens when part of the transmitted signals from satellite is reflected by the earth surface or any surface that have high power of reflection before the signals reach to the receiver. This scenario also happen when the receiver received more secondary path signal from various directions, which is neither coded translated nor understandable by GPS receiver and resulted from reflection from earth surface or any high objects for instance buildings around the observation station [19].

The number of visible satellites, the geometry of the satellite combination and the condition of the visible signals determine the positioning conditions. The task of choosing the satellite combination under the prevailing conditions is called satellite selection. Satellite selection analysis is complex because, depending on the geometry of the satellite combination as seen from the receiver, some satellite signals are more valuable than the others and PR errors vary with time [20].

The selective availability (SA) is the deliberate degradation by the US Defense Department of the GPS signals to deny non-authorized users certain levels of accuracy otherwise possible with unclassified C/A-code receivers. When the SA was implemented it causes error order of the 100 m. US Government has turned off the SA a few minutes past midnight eastern daylight time after the end of May 1, 2000. Since then, civilian users of GPS will be able to pinpoint locations up to ten times more accurately then they did before [21].

These overview discussions on GPS error sources and magnitudes, as well as the effects of satellite geometry, are summarized in Table 1.

Table 1 GPS error source and their magnitudes in meter [21]

Error source	Error magnitude	
	SA on	SA off
Selective availability	24.0	0.0
Ionospheric delay	7.0	7.0
Tropospheric delay	0.2	0.2
Clock and ephemeris	2.3	2.3
Receiver noise	0.6	0.6
Multipath	1.5	1.5
User equivalent range error (UERE)	25.0	7.5
Typical horizontal DOP (HDOP)	1.5	1.5
Stand-alone horizontal accuracy (95 %)	±75.0	±22.5

3 Wavelet De-noise Fundamental Principle

A one-dimensional model of signals with additive noises can be shown as $Y = X + e$, where Y and X denote noise-containing and de-noised signals, respectively. Also, e is a noise. After decomposing the data Y by the discrete wavelet transform (DWT), we get the coefficients y_n. In the wavelet domain, the problem can be formulated as $y_n = x_n + e_n$, where y_n are noisy wavelet coefficients, x_n are true coefficients and e_n are independent noise coefficients. A simple de-noising algorithm via WT consists of three steps: decompose the noisy signal by WT, de-noise the noisy wavelet coefficients according to some rules and take the inverse WT from the de-noised coefficients [22].

The DWT decomposes the signal $S(t)$ into an approximate component and several detailed components:

$$S(t) = A_j(t) + \sum_{j \in J} D_j(t) \tag{2}$$

where

$$A_j(t) = \sum_{k \in Z} c_{j,k} \varphi_{j,k}(t); c_{j,k} = \left\langle S(t), \varphi_{j,k}(t) \right\rangle \tag{3}$$

and

$$D_j(t) = \sum_{k \in Z} d_{j,k} \psi_{j,k}(t); d_{j,k} = \left\langle S(t), \psi_{j,k}(t) \right\rangle \tag{4}$$

where J is the total level of DWT, A_j is the approximate component at level j and D_j is the detailed component at level j. $c_{j,k}$ is the wavelet coefficient of A_j and is obtained by the inner product of spectrum $S(t)$ and the scaling function $\varphi_{j,k}$ at the level j with translation k. Similarly, $d_{j,k}$ is wavelet coefficients of D_j and is calculated using the inner product of spectrum $S(t)$ and the wavelet function $\psi_{j,k}$ at level j with translation k. As level j increases the wavelet $\psi_{j,k}$ and scaling function $\varphi_{j,k}$ stretches by a factor of two. Also, as k increases, the wavelet shifts right [23].

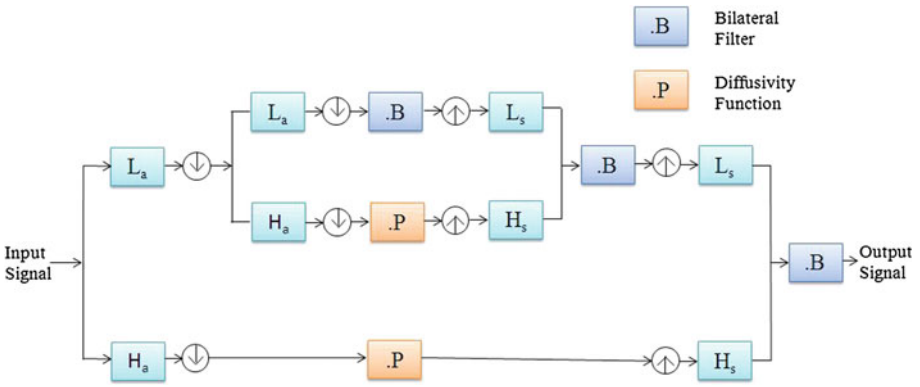

Fig. 1 Illustration of the proposed method

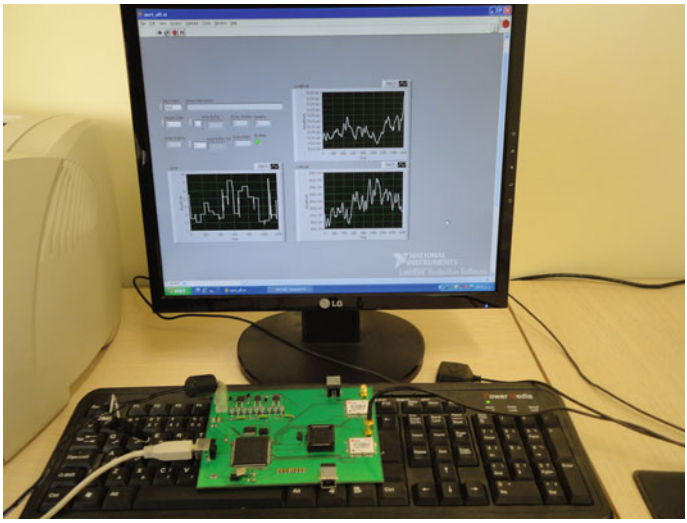

Fig. 2 Schematics of hardware implementation in this study

4 A Multiresolution Signal De-noising Framework

Noise may have low-frequency (coarse-gain) and high-frequency (fine-gain) fluctuations. High-frequency noise is relatively easier to remove; on the other hand, it is difficult to distinguish between real signal and low-frequency noise. Multiresolution analysis has been proven to be an important tool for eliminating noise in signal. It is possible to distinguish between noise and signal information better at one resolution level than another [24]. The proposed framework is illustrated in Fig. 1.

GPS data signal is decomposed into two-set of coefficients, low-frequency and high-frequency via convolving the input signal with low-pass (L) and high-pass (H) filter, respectively. A downsampling processing is then performed after the convolution. As the signal reconstructed back; BF is applied to the approximation subbands. Unlike the standard single-level BF [7], this multiresolution BF has the potential of eliminating low-frequency noise components. The high-frequency component generated at each resolution is then processed by a

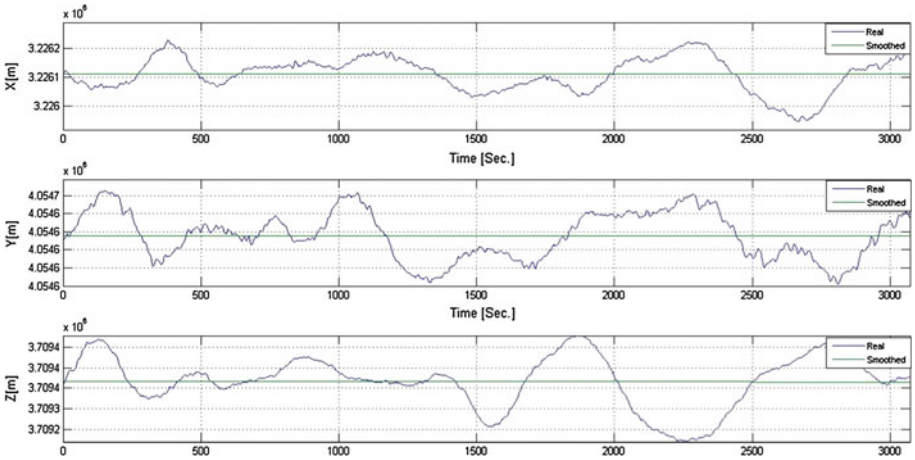

Fig. 3 X, Y and Z of real and smoothed using the proposed algorithm based on Haar wavelet (SA on)

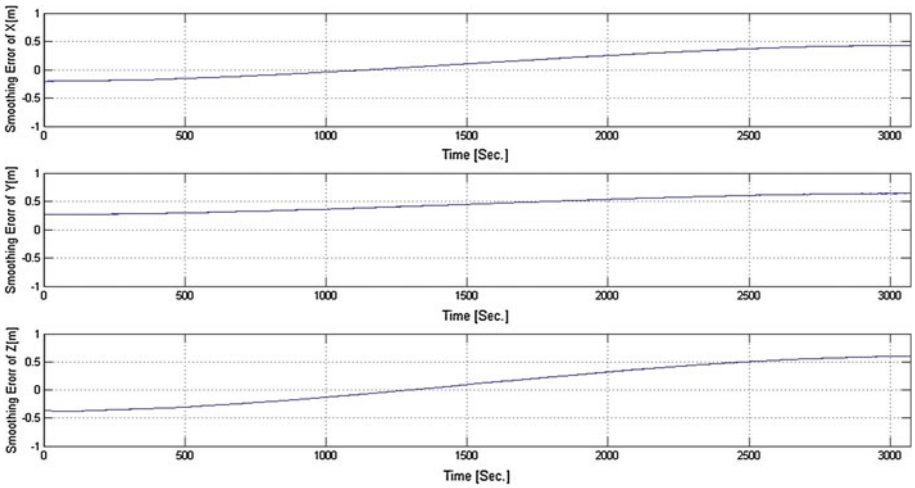

Fig. 4 Smoothing errors of X, Y and Z using the proposed algorithm based on Haar wavelet (SA on)

non-linear operator which can decrease the magnitude of noises and retain the useful data. The signal reconstruction process can be achieved by adding the processed high-frequency component and the processed low-frequency component at the lowest resolution to form the low-frequency component of the second lowest resolution. Then bilateral filtering is applied to approximate this level and after that combined with the processed high-frequency component at the same resolution to form the low-frequency part of the resolution one level up. The process is repeated until the original signal is reconstructed.

The BF takes a weighted sum of the samples in a local neighborhood; the weights depend on both the spatial distance and the signal value distance. In this way, sharp features are preserved well while noise is averaged out. Mathematically, at a sample location x and its neighborhood sample y, the output of the BF is calculated as follows [25]:

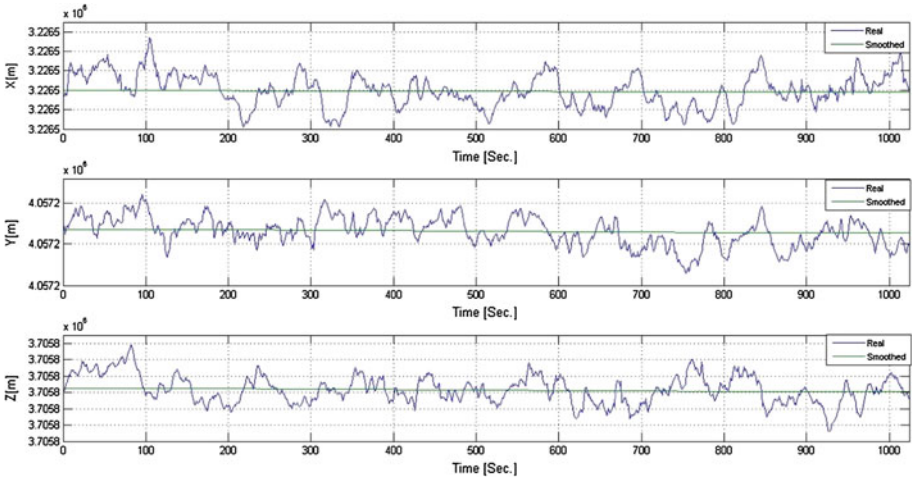

Fig. 5 X, Y and Z of real and smoothed using the proposed algorithm based on Haar wavelet (SA off)

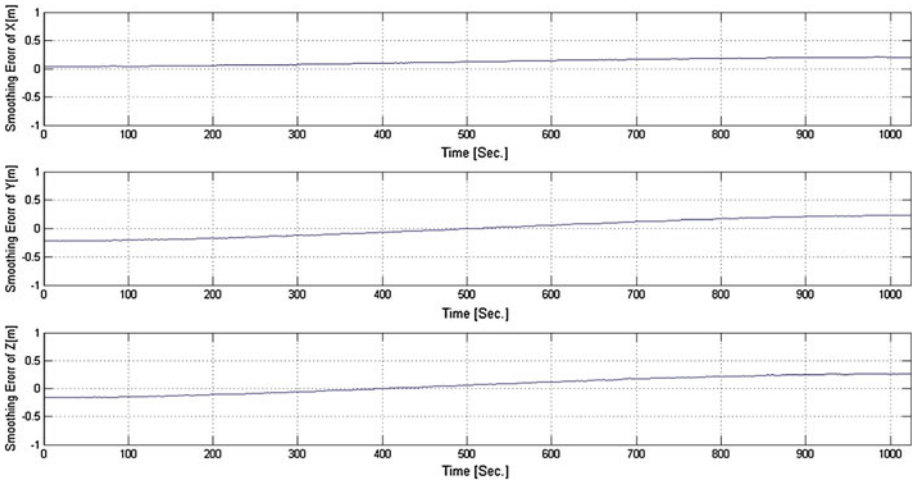

Fig. 6 Smoothing errors of X, Y and Z using the proposed algorithm based on Haar wavelet (SA off)

$$\tilde{f}(X) = \frac{1}{C} \sum_{y \varepsilon \mathrm{N}(x)} e^{\frac{-\|y-x\|^2}{2\sigma_d^2}} e^{\frac{-|f(y)-f(x)|^2}{2\sigma_r^2}} f(y) \tag{5}$$

where σ_d and σ_r are parameters controlling the fall-off of the weights in spatial and signal value domains, respectively, $N(x)$ is a spatial neighborhood of x and C is the normalization constant [25].

$$C = \sum_{y \varepsilon \mathrm{N}(x)} e^{\frac{-\|y-x\|^2}{2\sigma_d^2}} e^{\frac{-|f(y)-f(x)|^2}{2\sigma_r^2}} \tag{6}$$

The extent of smoothing can be controlled by the σ_d value. The larger the σ_d value is, the wider the extent of smoothing can be. The discontinuity can be controlled by the σ_r

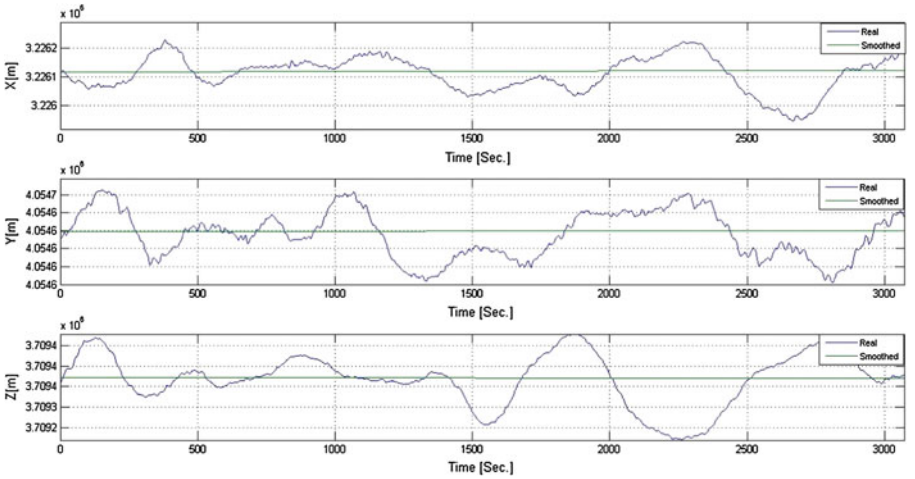

Fig. 7 X, Y and Z of real and smoothed using the proposed algorithm based on Meyer wavelet (SA on)

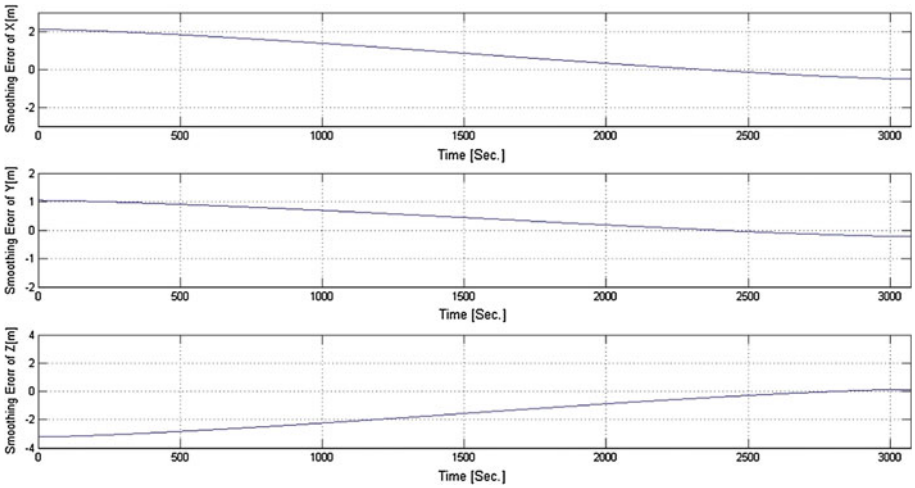

Fig. 8 Smoothing errors of X, Y and Z using the proposed algorithm based on Meyer wavelet (SA on)

value. When the σ_r value is less than the discontinuity amount, the filter is basically useless against eliminating the discontinuity. When σ_r is larger than the discontinuity amount, the discontinuity can be eliminated.

The behavior of the bilateral filter depending on the derivative of the input signal and $\frac{\sigma_r}{\sigma_d}$ values was analyzed. We provide an empirical study for parameters optimal values. It can be seen that the signal domain parameter σ_r is more critical than the spatial domain parameter σ_d. It appears that a good range for the value σ_d is roughly [1.3–2.4]. For the value σ_r, $\sigma_r = 2 \times \sigma_d$ is a better choice.

Non-linear diffusion has deservedly attracted much attention in the field of signal processing for its ability to reduce noise while preserving (or even enhancing) important features of the signal. Non-linear diffusion creates a family of restored signals $\tilde{f}$ by starting from the noisy signal f and evolving it locally according to a process described by a non-linear

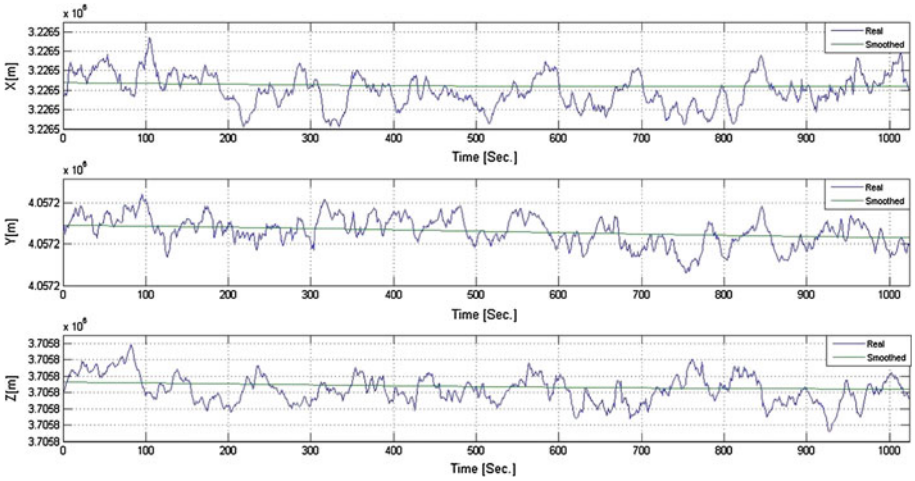

Fig. 9 X, Y and Z of real and smoothed using the proposed algorithm based on Meyer wavelet (SA off)

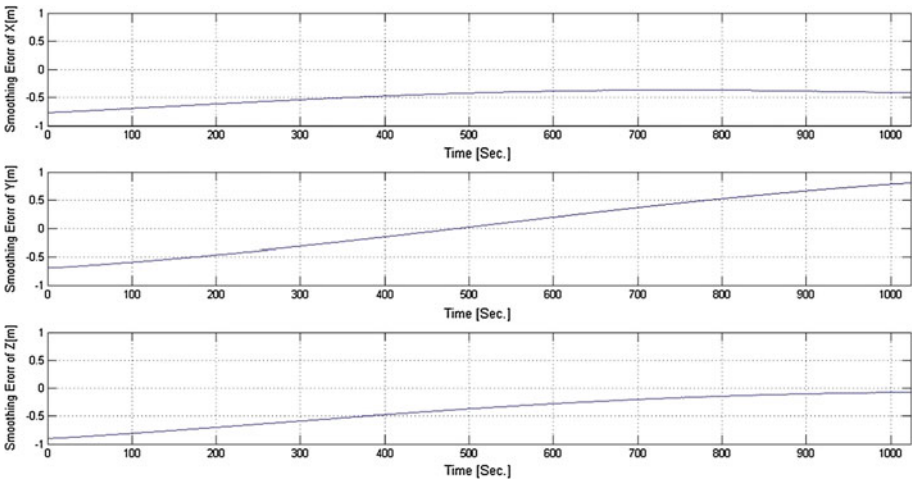

Fig. 10 Smoothing errors of X, Y and Z using the proposed algorithm based on Meyer wavelet (SA off)

partial differential equation. This process is controlled by a diffusivity function $C[l]$ of the signal gradient. Typically, $C[l]$ is a non-negative, non-increasing function of the gradient magnitude, approaching zero as $l \to \infty$. This setting leads to the effect that smoothing of $\tilde{f}$ proceeds faster in homogeneous regions (where the gradient is small, caused possibly by noise), and discontinuities (large gradient, hopefully corresponding to important features of the underlying signal) tend to be preserved [26].

At scale 2^j, the two filtering and downsampling operation can be expressed by:

$$A_k^{(j)} = \sum_{l \in Z} L_a[l - 2k] A_l^{(j-1)} \tag{7}$$

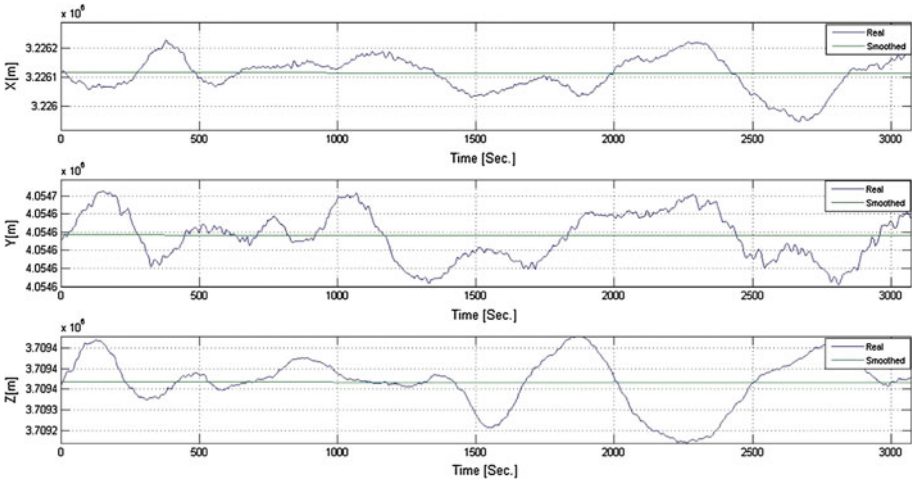

Fig. 11 X, Y and Z of real and smoothed using the proposed algorithm based on Coiflet wavelet (SA on)

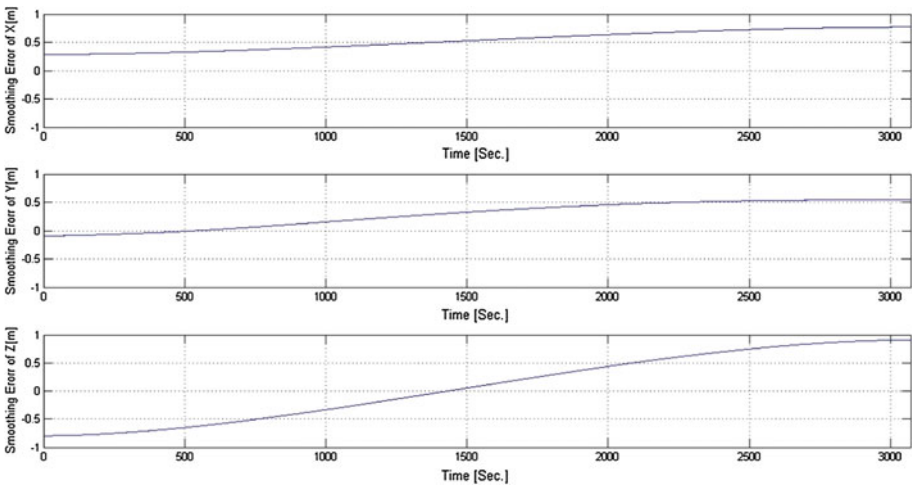

Fig. 12 Smoothing errors of X, Y and Z using the proposed algorithm based on Coiflet wavelet (SA on)

and

$$D_k^{(j)} = \sum_{l \in \mathrm{Z}} H_a[l - 2k] D_l^{(j-1)} \tag{8}$$

where L_a is the low-pass, H_a is high-pass filter, A^j is approximation coefficient and D^j is detail coefficient. The reconstruction formula for each layer becomes:

$$A_k^{(j)} = \sum_{l \in \mathrm{Z}} B[l] A_l^{(j+1)} L_s[k - 2l] + P[l] D_l^{(j+1)} H_s[k - 2l] \tag{9}$$

where L_a and L_s (H_a and H_s) are respectively conjugate at scale 2^j, $B[l]$ is the BF that depending on the value of A^{j+1} and $P[l]$ depending on the absolute value of D^{j+1} ($0 \leq$

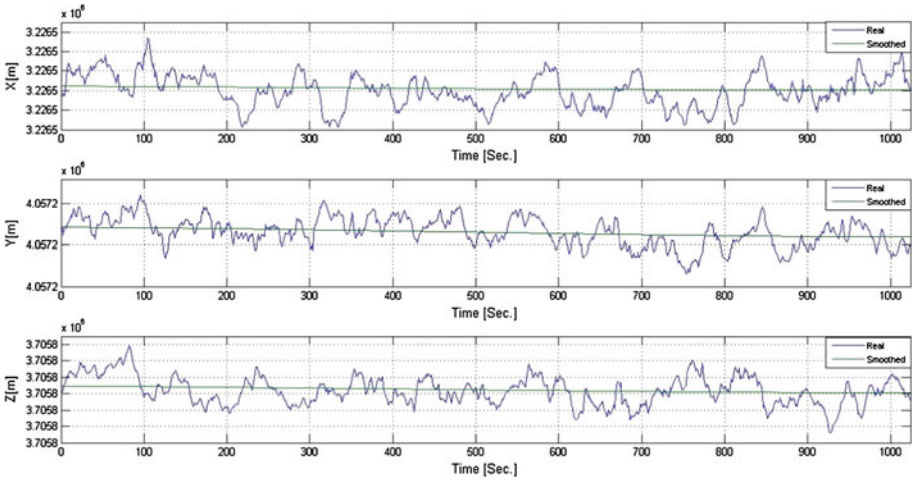

Fig. 13 X, Y and Z of real and smoothed using the proposed algorithm based on Coiflet wavelet (SA off)

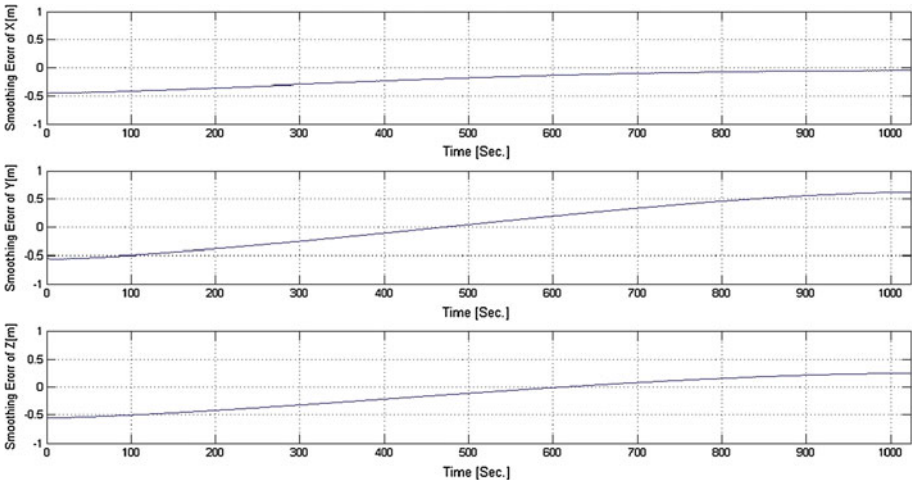

Fig. 14 Smoothing errors of X, $Y and Z$ using the proposed algorithm based on Coiflet wavelet (SA off)

$P[l] \leq 1$ and $P[l] = 1 - C[l]$, where $C[l]$ is the diffusivity function). The diffusivity function used was the one proposed by Weickret [27] as:

$$C[|l|] = \begin{cases} 1 & ; |l| = 0, \\ 1 - \exp(\frac{-3.31488}{(\frac{|l|}{\lambda})^8}) & ; |l| \rangle 0, \end{cases} \tag{10}$$

where l in equation above is detail coefficient at scale 2^j and λ is a constant for serving as threshold of gradient size. Before the wavelet decomposition, the input signal range has been changed to [0,1] scale. Optimal range λ for de-noise components of the detail coefficients is roughly [0.01–0.004].

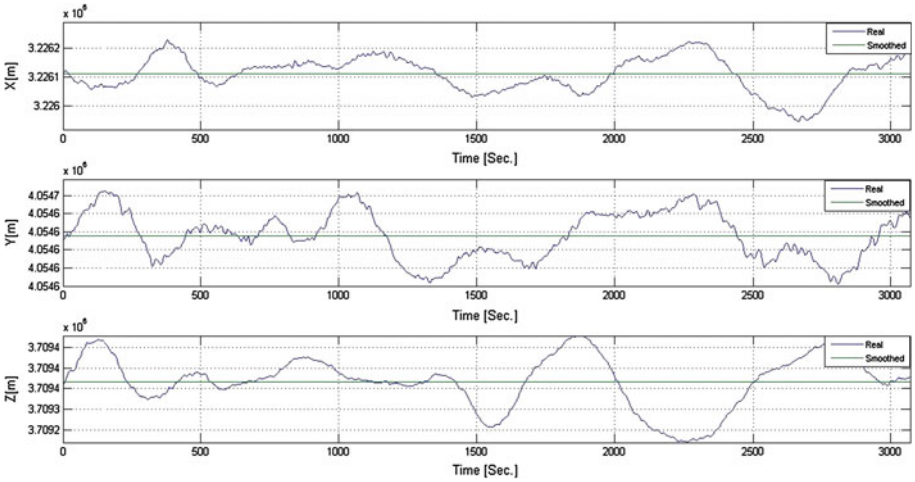

Fig. 15 X, Y and Z of real and smoothed using the proposed algorithm based on Daubechie wavelet (SA on)

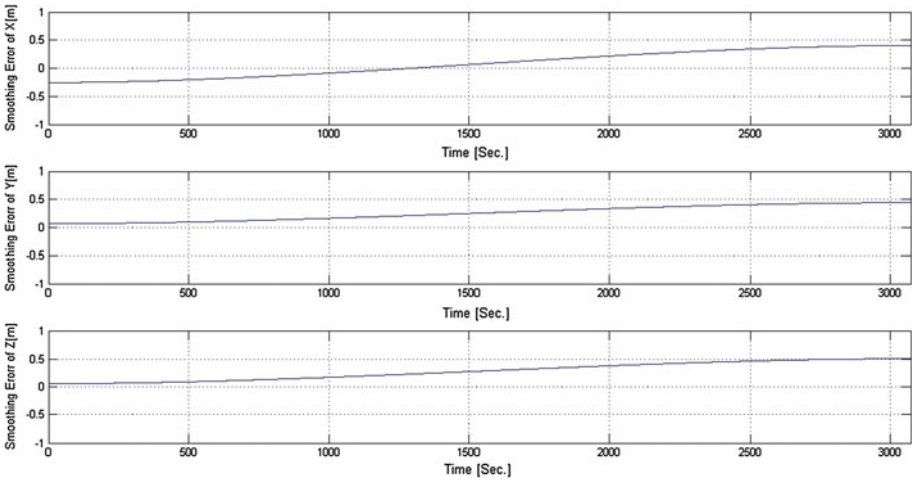

Fig. 16 Smoothing errors of X, Y and Z using the proposed algorithm based on Daubechie wavelet (SA on)

5 Hardware and Software Implementation

To verify the validity of the proposed approach, a practical data analysis was carried out. The data was collected at sample rate of one second in building of Computer Control and Fuzzy Logic Research Lab in the Iran University of Science and Technology. A GPS receiver manufactured by Rockwell Company was used. The Rockwell microtraker low-power receiver was a five-channel and L1 C/A-code receiver [28]. Real data collecting has been in two different periods, before and after turning off the SA (before and after 1st May 2000). Figure 2 shows schematics of hardware implementation in this research.

The hardware platform consists of a computer in which the software resides, one RS232 port to interface with a GPS receiver and additional Input-Output (I/O) interface to connect to other hardware devices. The software deals with data processing, systems controls and the

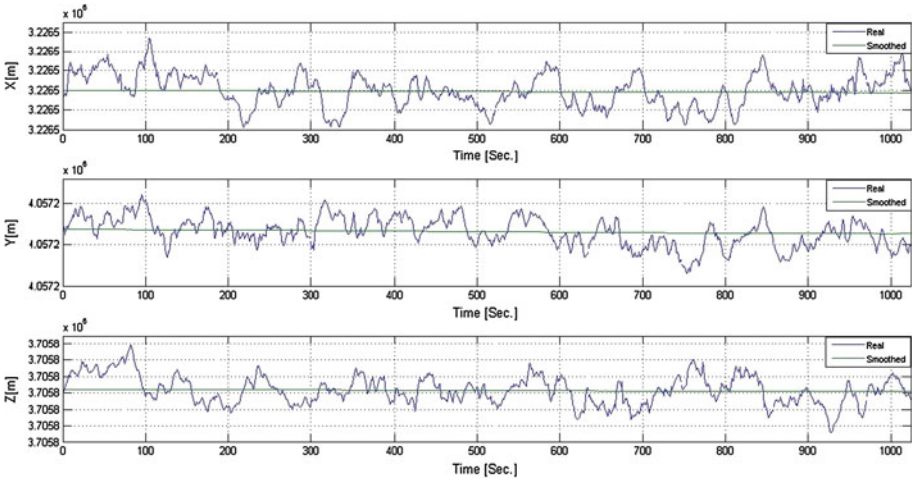

Fig. 17 X, Y and Z of real and smoothed using the proposed algorithm based on Daubechie wavelet (SA off)

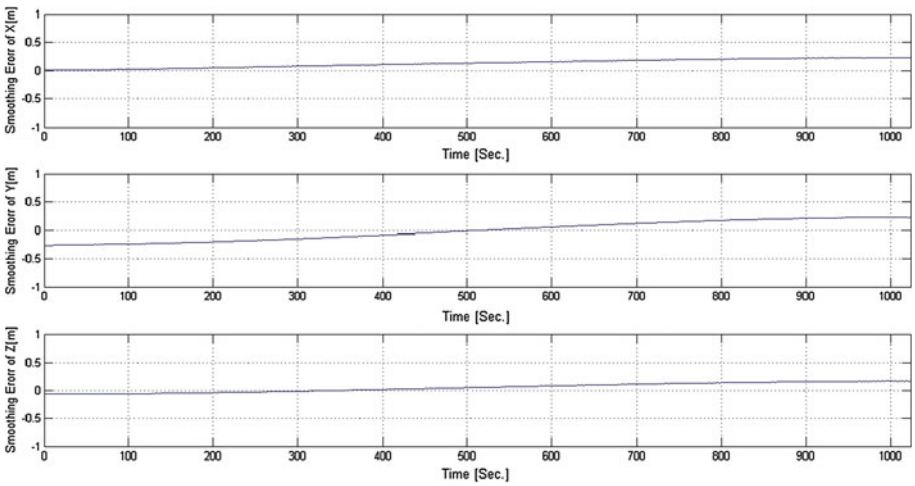

Fig. 18 Smoothing errors of X, Y and Z using the proposed algorithm based on Daubechie wavelet (SA off)

communication operations. GPS data is received from the GPS receiver via GPS RS232 port and is smoothed by software in the computer. The GPS receiver uses TTL signal standard in communication, while the computer uses RS232 to communicate with the serial device. Therefore the MAX chip is required for signals converter.

The I/O devices will be controlled by software. The implementation of all communication processes and data processing will all be done by software. There are several commands that can be sent. These include commands to change the device settings, the required setting parameters and commands to control attached peripherals.

Some experimental results are given in the following. The optimal selection of proposed method parameters was based on the experimental results. Increasing the order of algorithm improves the proposed algorithm performance. Increasing the order of algorithm increases the memory for software implementation and also the structure complexity for hardware

Table 2 Position smoothing errors using Haar, Meyer, Coiflet and Daubechie wavelets with SA on (in m)

Wavelet type	Parameters	X Component	Y Component	Z Component
Haar	Max	0.4326	0.6409	0.5958
	Min	−0.2040	0.2672	−0.3781
	Average	0.1147	0.4542	0.1101
	RMS	0.2471	0.4720	0.3531
Meyer	Max	2.1061	1.0445	0.1439
	Min	−0.5072	−0.2247	−3.2279
	Average	0.8059	0.4171	−1.5268
	RMS	1.1665	0.5846	1.8748
Coiflet	Max	0.7693	0.5459	0.9077
	Min	0.2829	−0.0921	−0.7983
	Average	0.5312	0.2862	0.0716
	RMS	0.5565	0.3627	0.5873
Daubechie	Max	0.4021	0.4401	0.5081
	Min	−0.2637	0.0630	0.0581
	Average	0.0688	0.2511	0.2829
	RMS	0.2397	0.2828	0.3229

Table 3 Position smoothing errors using Haar, Meyer, Coiflet and Daubechie wavelets with SA off (in m)

Wavelet type	Parameters	X Component	Y Component	Z Component
Haar	Max	0.2015	0.2239	0.2641
	Min	0.0369	−0.2281	−0.1608
	Average	0.1209	−0.0021	0.0602
	RMS	0.1337	0.1558	0.1596
Meyer	Max	−0.3702	0.8013	−0.0725
	Min	−0.7685	−0.6937	−0.8984
	Average	−0.4841	0.0462	−0.4063
	RMS	0.4996	0.4705	0.4832
Coiflet	Max	−0.0584	0.6228	0.2468
	Min	−0.4448	−0.5664	−0.5551
	Average	−0.2114	0.0466	−0.1214
	RMS	0.2471	0.3968	0.2914
Daubechie	Max	0.2145	0.2357	0.1806
	Min	0.0458	−0.2495	−0.0694
	Average	0.1331	−0.0046	0.0577
	RMS	0.1452	0.1672	0.1036

implementation. Therefore, a trade-off in selecting the order of algorithm between CPU time and accuracy of methods is required. The number of decomposition levels is four levels for the SA on and five levels for the SA off. Figures 3, 4, 5, 6, 7, 8, 9, 10, 11, 12, 13, 14, 15, 16,

Table 4 Comparing position smoothing accuracy using Haar, Meyer, Coiflet and Daubechie wavelets with and without SA (in m)

Wavelet type	Total RMS (SA on)	Total RMS (SA off)
Haar	0.3690	0.1501
Meyer	1.3188	0.4846
Coiflet	0.5119	0.3180
Daubechie	0.2838	0.1412

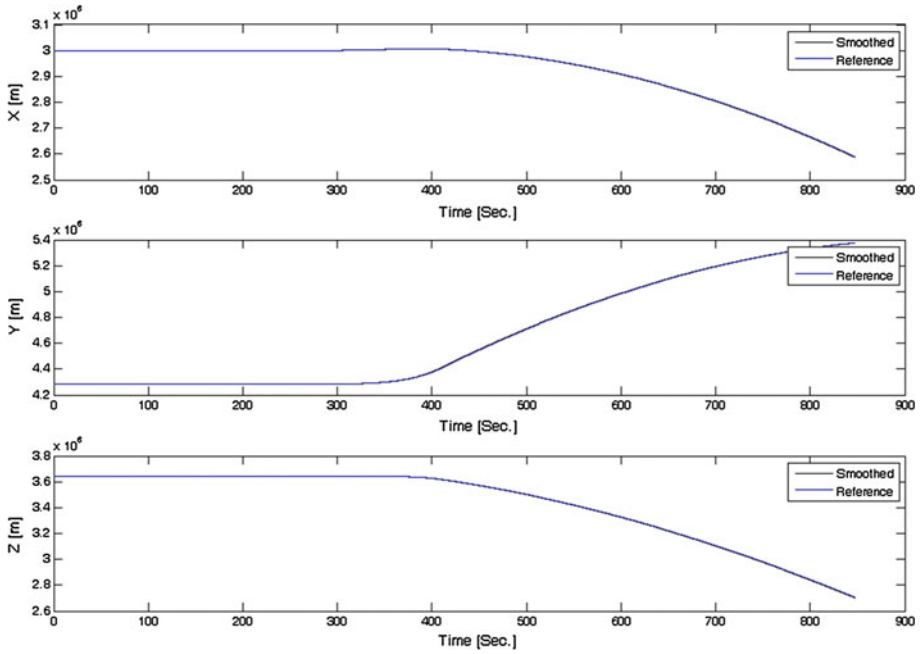

Fig. 19 X, Y and Z of reference and smoothed using the proposed algorithm

17 and 18 plot X, Y and Z smoothing for test data using the proposed algorithm, before and after SA, respectively.

Tables 2 and 3 show smoothing errors statistical significance characteristics for 1,000 positioning test data, with and without SA, respectively.

For the performance evaluating of the proposed method, Root Mean Square Error (RMSE) was used as [29–31]:

$$RMS = \sqrt{\frac{1}{T}\sum_{i=1}^{i=T}[s(i) - \tilde{s}(i)]^2} \tag{11}$$

where T is number of tests and $s(i)$ and $\tilde{s}(i)$ represent the clean data and de-noised data, respectively. Table 4 shows the comparing position smoothing accuracy using four proposed methods, with and without SA.

Table 4 shows that total RMSE reduces to less than 0.29 m with SA on and 0.15 m with SA off using Daubechie wavelet. Table 4 demonstrates that position smoothing using the

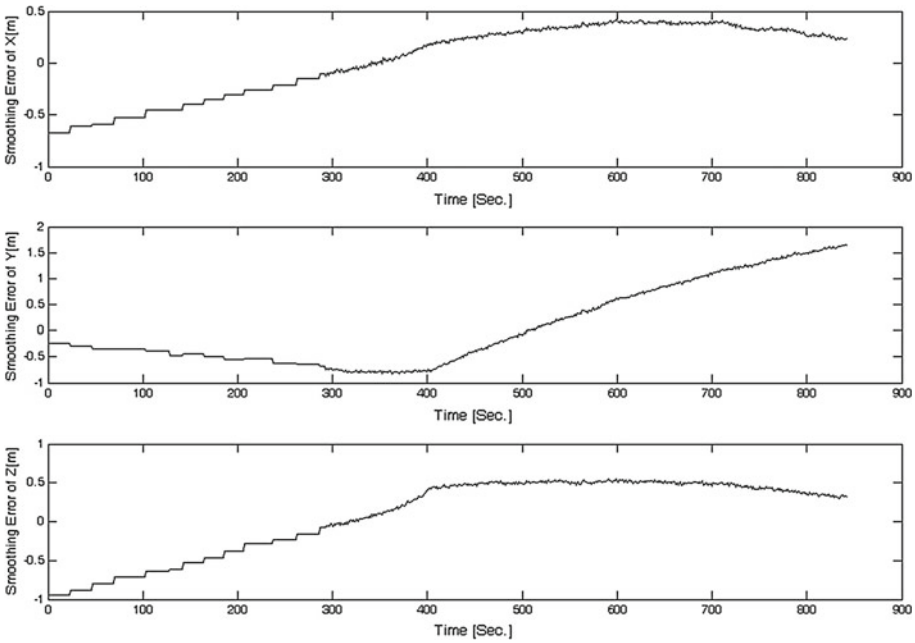

Fig. 20 Smoothing errors of X, Y and Z using the proposed algorithm

proposed algorithm based on Daubechie wavelet has better accuracy; since position smoothing RMSE in Daubechie wavelet is lower than other wavelets. In proposed algorithm, quality of the results obtained is very good even under the SA conditions.

A kinematic dataset was used to illustrate the performance of the proposed smoothing method for high dynamic platforms such as airplane. We achieved high performance in terms of position accuracy by tuning the filter parameters. The results from processing of data showed about one meter level accuracy, which is close to that of real-time standalone dual-frequency point positioning. For kinematic data testing, Figs. 19 and 20 plot X, Y and Z smoothing and their smoothing errors using the proposed algorithm, respectively.

There are only few papers (for examples [13,18,32]) that smooth GPS receiver positioning data without any extra sensor. The proposed method in this paper has more accuracy than them, since RMS error of smoothing in this method is very lower than other methods. Also, it is very accurate than our previous papers such as reference of [32].

6 Conclusion

The GPS represents one of the main systems for navigation aids. PR measurements are influenced by many factors, including satellite clock bias, SA policy, ionosphere delay, troposphere delay, multipath delay, hot noise and others. These errors can seriously reduce the precision and reliability of GPS positioning when remained in GPS data. The WT was used as a powerful tool to separate systematic errors from the signal. In this paper, we have presented a new method for effective removal of GPS receiver positioning data noise using WT, BF and diffusivity function. Theoretical analysis and practical calculation proved applicability of the proposed approach. The experimental results on the collected data from a single-frequency GPS receiver demonstrate that the proposed method can effectively improve the GPS

positioning precision; so that the total RMS error reduced to less than 0.29 m with SA on and 0.15 m with SA off using Daubechie wavelet.

Acknowledgments The authors would like to thank industry, for their valuable support during the authors' research work.

References

1. MacDonald, J. T., Ucci, D. R., & LoCicero, J. L. (2008). Isolating multi-path effects from the position estimate residuals in GPS receivers. In *IEEE conference on military communications*, pp. 1–6.
2. Fang, B. T. (1990). Simple solutions for hyperbolic and related position fixes. *IEEE Transactions on Aerospace and Electronic Systems, 26*(5), 748–753.
3. Koyama, Y., Liang, T. K., & Tanaka, T. (2009). High-precision GPS measurement for motorcycle trajectory using Kalman filter. In *IEEE conference on networked sensing systems*, pp. 1–4.
4. Zhu, Z. S., Lu, D. J., & Wang, Q. (2008). Study on nerve-cell based real-time estimation method for gps multi-path error. In *IEEE conference on machine learning and cybernetics*, pp. 1455–1460.
5. Shaw, M., Sandhoo, K., & Turner, D. (2000). Modernization of the global positioning system. *GPS World, 11*(9), 36–44.
6. Qiang, Q., Jiliu, Z., Kun, H., & Jian, L. (2005). Noise reduction based on wavelet transform under non-stationary environments. In *IEEE conference on mechatronics and automation*, pp. 2123–2129.
7. Tomasi, C., & Manduchi, R. (1998). Bilateral filtering for gray and color images. In *IEEE conference on computer vision*, pp. 839–846.
8. Anand, C. Sh., & Sahambi, J. S. (2008). MRI denoising using bilateral filter in redundant wavelet domain. In *IEEE Conference on TENCON 2008*, pp. 1–6.
9. Lee, H. K. (2002). Time-propagated measurement fusion and its application to multipath detection and isolation, PhD dissertation, School of Electrical Engineering and Computer Science, Seoul National University.
10. Hatch, R. R. (1982). The synergism of GPS code and carrier measurements. In *Proceedings of the third international geodetic symposium on satellite doppler positioning* (Vol. 2, pp. 1213–1232).
11. Hwang, P. Y. C., & Brown, R. G. (1990). GPS Navigation: Combining pseudorange with continuous carrier phase using a Kalman filter. *Journal of the Institute of Navigation, 37*(2), 181–196.
12. Bisnath, S. B., & Langley, R. B. (1999). Precise, efficient GPS-based geometric tracking of low earth orbiters. In *Proceedings of the institute of navigation annual meeting*, pp. 751–760.
13. Ford, T. J., & Hamilton, J. (2003). A new positioning filter: Phase smoothing in the position domain. *Journal of the Institute of Navigation, 50*(2), 65–78.
14. Lee, H. K., Rizos, C., & Jee, G. I. (2004). Design of kinematic DGPS filters with consistent error covariance information. *IEE Proceedings on Radar, Sonar and Navigation, 151*(6), 382–388.
15. Lee, H. K., & Rizos, C. (2008). Position-domain hatch filter for kinematic differential GPS/GNSS. *IEEE Transactions on Aerospace and Electronic Systems, 44*(1), 30–40.
16. Nunes, F. D., Leitão, J. M. N., & Sousa, F. M. G. (2009). Nonlinear filtering in GNSS pseudorange dynamics estimation combining code delay and carrier phase. *IEEE Journal of Selected Topics in Signal Processing, 3*(4), 639–650.
17. Kaplan, E. D. (1996). *Understanding GPS: Principle and applications*. Boston: Artech House Publishers.
18. Thipparthi, S. N. (2004). *Improving positional accuracy using carrier smoothing techniques in inexpensive GPS receivers*, M.S. Thesis, New Mexico State University.
19. Kamarudin, N., & Amin, Z. M. (2004). Multipath error detection using different GPS receiver's antenna. In *3rd FIG regional conference*, pp. 1–11.
20. Wu, C. H., Su, W. H., & Ho, Y. W. (2010). A study on GPS GDOP approximation using support-vector machines. *IEEE Transactions on Instrumentation and Measurement, 60*(1), 137–145.
21. Alkan, R. M., & Arslan, E. (2002). GPS standard positioning service performance after selective availability turned off. In *International Symposium on GIS*, pp. 1–9.
22. Lilong, L., Hongyan, W., & Bin, L. (2010). Mitigation of systematic errors of gps positioning based on wavelet denoise. In *Second WRI global congress on intelligent systems*, pp. 253–255.
23. Du, P., Lin, S. M., Kibbe, W. A., & Wang, H. (2007). Application of wavelet transform to the ms-based proteomics data preprocessing. In *IEEE conference on bioinformatics and bioengineering*, pp. 680–686.

24. Zang, M., & Gunturk, B. K. (2008). Multiresolution bilateral filtering for image denoising. *IEEE Transactions on Image Processing, 17*(12), 2324–2333.
25. Mustafa, Z. A., & Kadah, Y. M. (2011). Multi resolution bilateral filter for MR image denoising. In *IEEE conference on biomedical engineering*, pp. 180–184.
26. Mrazek, P., Weickert, J., & Steidl, G. (2003). Correspondences between wavelet shrinkage and nonlinear diffusion. *Lecture Notes in Computer Science, 2695*, 101–116.
27. Weickert, J., ter Romeny, B. M., & Viergever, M. A. (1998). Efficient and reliable schemes for nonlinear diffusion filtering. *IEEE Transactions on Image Processing, 7*(3), 398–410.
28. Zodiac GPS Receiver Family Designer's Guide. Rockwell Semiconductor Systems, GPS-33. (1996).
29. Vizireanu, D. N. (2011). A simple and precise real-time four point single sinusoid signals instantaneous frequency estimation method for portable DSP based instrumentation measurement. *Journal of Measurement, 44*(2), 500–502.
30. Azami, H., Mosavi, M. R., & Sanei, S. (2012). Classification of GPS satellites using improved back propagation training algorithms. *Journal of Wireless Personal Communications* doi:10.1007/s11277-012-0844-7.
31. Reis, J., Sanguino, J., & Rodrigues, A. (2012). Baseline influence on single-frequency GPS precise heading estimation. *Journal of Wireless Personal Communications, 64*, 185–196.
32. Mosavi, M. R. (2009). GPS data smoothing. *Journal of Remote Sensing, 22*, 21–35.

Author Biographies

M. R. Mosavi received his B.S., M.S., and Ph.D. degrees in Electronic Engineering from Department of Electrical Engineering, Iran University of Science and Technology (IUST), Tehran, Iran in 1997, 1998, and 2004, respectively. He is currently faculty member of Department of Electrical Engineering of IUST as associate professor. He is the author of about 150 scientific publications on journals and international conferences. His research interests include Artificial Intelligent Systems, Global Positioning Systems, Geographic Information Systems and Remote Sensing.

I. EmamGholipour received his B.S. degree in Electronic Engineering from Department of Electrical and Computer Engineering, Mazandaran University, Babol, Iran in 2009. He is currently master science student of Department of Electrical Engineering of IUST. His research interests include Signal Processing.